Reprinted by permission from IEEE TRANSACTIONS ON ANTENNAS AND PROPAGATION
Vol. AP-21, No. 4, July 1973, pp. 435–445

Probe Compensated Near-Field Measurements on a Cylinder

W. MARSHALL LEACH, JR., AND DEMETRIUS T. PARIS

Abstract—**A new method is developed for determining the far-field pattern of an antenna from probe compensated near-field measurements over the surface of a right circular cylinder enclosing the antenna. The method is derived by first expanding both the field radiated by the antenna and the field radiated by the measurement probe, when it is used as a transmitter, into cylindrical wave expansions. The Lorentz reciprocity theorem is then used to solve for the field radiated by the antenna from the probe output voltage. It is shown rigorously that the antenna pattern can be determined independently of the characteristics of the measurement probe provided that certain calibration data are known. A method for determining these data from the measured far field radiated by the probe is described. It is shown that the necessary numerical integration can be performed with the fast Fourier transform algorithm. Experimental results are presented to validate the theory and to demonstrate its practicality from a measurement and computational viewpoint.**

I. Introduction

THIS PAPER concerns with the problem of the determination of the far-field pattern of an antenna from measurements made in the near field. This problem has been one of considerable interest [1]–[7], particularly in the case of microwave antennas for which the distance to the far field exceeds the dimensions of available antenna test ranges. Early work in this area was based on the assumption that the measurement probe did not disturb the field and that it measured the field at a point. The far-field calculations were usually based on scalar diffraction theory.

There have been two recent methods proposed which are based on three-dimensional modal expansions of the antenna fields and which remove the ideal probe assumption. A technique based on the plane wave spectrum expansion has been proposed by Kerns [1] to predict the far-field pattern from near-field data measured over the surface of a plane located in front of the antenna. A method was described to compensate for the effects of the measurement probe using the measured far field of the probe when it is used as a transmitter. This work has been verified experimentally by Baird *et al.* [2]. Jensen [6] has described a method based on spherical wave expansions for obtaining the far field from near-field data measured over the surface of a sphere enclosing the antenna. However, the author implied that the method does not seem to be suitable for practical purposes unless an ideal probe is used. No experimental results were presented.

The method proposed in the present paper is based on the three-dimensional vector cylindrical wave expansion of an electromagnetic field. The approach is similar to that originally used by Brown and Jull [4] in that it is based on an application of the Lorentz reciprocity integral. It is shown that the complete vector far-field pattern of

Manuscript received September 22, 1972; revised January 5, 1973.
The authors are with the School of Electrical Engineering, Georgia Institute of Technology, Atlanta, Ga. 30332.

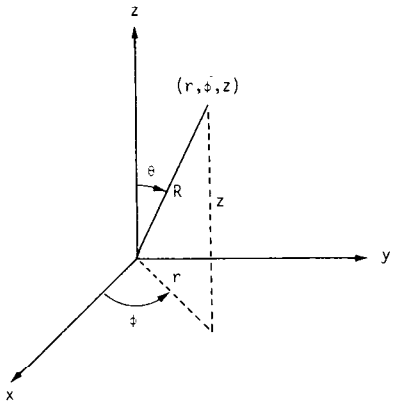

Fig. 1. Coordinate system definitions. (r indicates position vector of point (r, ϕ, z). Symbol caret over a coordinate symbol denotes unit vector in direction defined by increase in that coordinate.)

an arbitrary antenna can be obtained from near-field data measured over the surface of a cylinder enclosing the antenna. It is shown rigorously that the effects of the measurement probe can be compensated for if the complex amplitude weighting functions in the cylindrical wave expansion of the field radiated by the probe, when used as a transmitted, are known. It is shown that these weighting functions can be obtained from the measured amplitude and phase of the far field radiated by the probe.

II. Cylindrical Wave Expansion

In a linear, isotropic region containing no sources, it can be shown that the electric and magnetic field intensities can be expressed as functions of the cylindrical coordinates (r,ϕ,z) shown in Fig. 1 by linear combinations of the vectors $\boldsymbol{M}$ and $\boldsymbol{N}$ given by [8]

$$\boldsymbol{M}_{nh}^{i}(r) = \left(\hat{r}\frac{jn}{r}Z_n^i(\Lambda r) - \hat{\boldsymbol{\phi}}\frac{\partial Z_n^i}{\partial r}\right)\exp(jn\phi)\exp(-jhz) \tag{1}$$

$$\boldsymbol{N}_{nh}^{i}(r) = \left(-\hat{r}\frac{jh}{k}\frac{\partial Z_n^i}{\partial r} + \hat{\boldsymbol{\phi}}\frac{nh}{kr}Z_n^i(\Lambda r) + \hat{z}\frac{\Lambda^2}{k}Z_n^i(\Lambda r)\right) \cdot\exp(jn\phi)\exp(-jhz) \tag{2}$$

where n is any integer, h is any real number, $k = \omega(\mu\epsilon)^{1/2}$, and where $\Lambda = (k^2 - h^2)^{1/2}$ for $h \leq k$ and $-j(h^2 - k^2)^{1/2}$ for $h > k$. The function $Z_n^i(\Lambda r)$ is any one of the four cylindrical Bessel functions given by $Z_n^1(\Lambda r) = J_n(\Lambda r)$, $Z_n^2(\Lambda r) = Y_n(\Lambda r)$, $Z_n^3(\Lambda r) = H_n^{(1)}(\Lambda r)$, and $Z_n^4(\Lambda r) = H_n^{(2)}(\Lambda r)$.

In the present case, a solution for $\boldsymbol{E}$ is desired which is valid in the region external to the smallest cylinder containing all sources defined by $r \geq r_a$. In order for $\boldsymbol{E}$ to satisfy the radiation condition at infinity, the large argument asymptotic expansion of the cylindrical Bessel function must represent surfaces of constant phase which propagate in the positive radial direction. For time variations of the form $\exp(j\omega t)$, the only one of these functions which satisfies this condition is the Hankel function of the second kind $H_n^{(2)}(\Lambda r)$. The large argument asymptotic expansion of this function is

$$H_n^{(2)}(\Lambda r) \sim j^{n+1/2}\left(\frac{2}{\pi\Lambda r}\right)^{1/2}\exp(-j\Lambda r). \tag{3}$$

The most general linear combination of the vectors $\boldsymbol{M}$ and $\boldsymbol{N}$ will involve an integral over all real h and a sum over all integer n. Thus, in this case, the general solution for $\boldsymbol{E}$ can be written

$$\boldsymbol{E}(r) = \sum_{n=-\infty}^{\infty}\int_{-\infty}^{\infty}(a_n(h)\boldsymbol{M}_{nh}^4(r) + b_n(h)\boldsymbol{N}_{nh}^4(r))\,dh \tag{4}$$

where $a_n(h)$ and $b_n(h)$ are the complex amplitude weighting functions of the vectors $\boldsymbol{M}$ and $\boldsymbol{N}$, respectively. The corresponding solution for $\boldsymbol{H}$ follows from Faraday's law and is given by

$$\boldsymbol{H}(r) = \frac{-k}{j\omega\mu}\sum_{n=-\infty}^{\infty}\int_{-\infty}^{\infty}(b_n(h)\boldsymbol{M}_{nh}^4(r) + a_n(h)\boldsymbol{N}_{nh}^4(r))\,dh. \tag{5}$$

In general, the evaluation of (4) or (5) is a formidable task. However, a considerable simplification results if the field is to be evaluated in the far-field region of the source. To do this, the Hankel function and its first derivative are first replaced by their large argument asymptotic expansions. The resulting integrals can then be evaluated by the method of steepest descent. Although the evaluation is straightforward, it is involved [9]. The results are:

$$\boldsymbol{E}(r) = \frac{-2k\sin\theta\exp(-jkR)}{R}\sum_{n=-\infty}^{\infty}j^n \cdot\exp(jn\phi)(\hat{\boldsymbol{\phi}}a_n(k\cos\theta) + \hat{\boldsymbol{\theta}}jb_n(k\cos\theta)) \tag{6}$$

$$\boldsymbol{H}(r) = \frac{\hat{R}\times\boldsymbol{E}}{\eta} \tag{7}$$

where (R,θ,ϕ) are the spherical coordinates of the far-field point and $\eta = (\mu/\epsilon)^{1/2}$.

It can be seen that the far field is determined only by those values of $a_n(h)$ and $b_n(h)$ for which $-k \leq h \leq k$, since $|k\cos\theta| \leq k$. Thus it can be concluded that the part of the near field for which $|h| > k$ represents evanescent waves in the vicinity of the antenna which in no way influence the far-field structure except to the extent that they are necessary to support a particular current distribution on the antenna.

III. Determination of Far Field from Probe Compensated Near-Field Measurements

In Fig. 2, let Σ_a be a cylinder of radius r_a that contains an arbitrary test antenna connected to signal generator A. Denote the field radiated by the test antenna by $\boldsymbol{E}_a(r)$ and $\boldsymbol{H}_a(r)$. Let this field be incident on a probe antenna whose reference origin $0'$ is located at the point (r_0,ϕ_0,z_0). Let the probe be connected via a waveguide feeder to generator B. Denote the field radiated by the probe when generator B is activated by $\boldsymbol{E}_b(r')$ and $\boldsymbol{H}_b(r')$, where r'

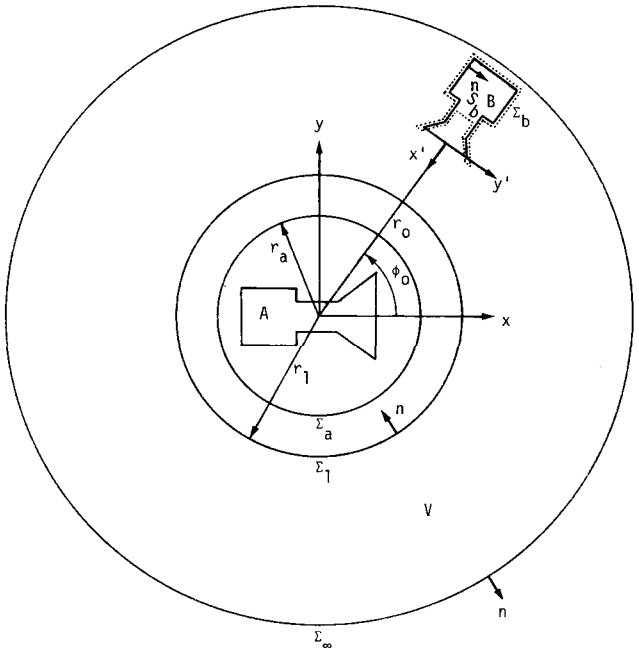

Fig. 2. Geometry for probe compensation derivation.

is measured with respect to 0'. Let the field scattered by the test antenna when generator B is activated be denoted by $\boldsymbol{E}_{as}(r)$ and $\boldsymbol{H}_{as}(r)$ and the field scattered by the probe when generator A is activated by $\boldsymbol{E}_{bs}(r')$ and $\boldsymbol{H}_{bs}(r')$. In the following analysis, it will be assumed that there are no multiply scattered fields between the test antenna and the probe so that the total scattered field is given by these terms.

It is desired to solve for the signal induced across the terminals of generator B when only generator A is activated. If generator B is then replaced by a linear detector having an input impedance equal to the output impedance of generator B, it will be shown that the far field of the test antenna can be calculated from the detector output voltage if its amplitude and phase are known as functions of ϕ_0 and z_0 over the cylinder of radius r_0. It will be assumed that the amplitude weighting functions in the cylindrical wave expansion of the field radiated by the probe when generator B is activated are known. Without loss of generality, it will be assumed that both generators A and B are matched to their respective waveguide feeders. Otherwise the theory holds with only slight modifications.

In Fig. 2, let V be the volume bounded by the surfaces Σ_1, Σ_b, and Σ_∞, where Σ_1 is the cylinder of radius r_1, Σ_b is the closed surface lying just outside the probe antenna and shield enclosing generator B which cuts the waveguide feeder for the probe at S_b, and Σ_∞ is the sphere of infinite radius. Since V contains no sources, it follows from the Lorentz reciprocity theorem that

$$\oint_{\Sigma_1+\Sigma_b+\Sigma_\infty} ((\boldsymbol{E}_a + \boldsymbol{E}_{bs}) \times (\boldsymbol{H}_b + \boldsymbol{H}_{as}) - (\boldsymbol{E}_b + \boldsymbol{E}_{as}) \times (\boldsymbol{H}_a + \boldsymbol{H}_{bs})) \cdot \hat{n}\, da = 0 \quad (8)$$

where all multiply scattered terms have been neglected. The integrand of this expression vanishes identically over Σ_∞ and over Σ_b except for the area S_b. Also, $\boldsymbol{E}_{bs} = 0$ and $\boldsymbol{H}_{bs} = 0$ over S_b by virtue of their definition. Thus it follows that (8) reduces to

$$\oint_{\Sigma_1} (\boldsymbol{E}_a \times \boldsymbol{H}_b - \boldsymbol{E}_b \times \boldsymbol{H}_a) \cdot (-\hat{r})\, da + \oint_{\Sigma_1} (\boldsymbol{E}_a \times \boldsymbol{H}_{as} - \boldsymbol{E}_{as} \times \boldsymbol{H}_a) \cdot (-\hat{r})\, da + \oint_{\Sigma_1} (\boldsymbol{E}_{bs} \times \boldsymbol{H}_b - \boldsymbol{E}_b \times \boldsymbol{H}_{bs}) \cdot (-\hat{r})\, da + \oint_{S_b} (\boldsymbol{E}_a \times \boldsymbol{H}_b - \boldsymbol{E}_b \times \boldsymbol{H}_a) \cdot (-\hat{x}')\, da = 0 \quad (9)$$

where the terms involving products of the scattered fields have been neglected and where it has been assumed that $\boldsymbol{E}_b + \boldsymbol{E}_{as} \cong \boldsymbol{E}_b$ and $\boldsymbol{H}_b + \boldsymbol{H}_{as} \cong \boldsymbol{H}_b$ over S_b. These assumptions are valid if the scattered fields over Σ_1 and S_b are small compared to the incident fields. Without them, the desired solution to (8) would be impossible.

Let the four integrals in (9) be denoted by I_1, I_2, I_3, and I_4, respectively. The integral for I_4 can be evaluated by assuming that the waveguide feeder for the probe will support only the dominant TE_{10} mode. (This is not a restrictive assumption, for the same result will be obtained for any other mode or combination of modes. Only the final constant of proportionality will differ.) The result is

$$I_4 = \frac{-1}{Z_w} C(r_0,\phi_0,z_0) \int_{-b/2}^{b/2} \int_{-a/2}^{a/2} 2\cos^2\left(\frac{\pi y'}{a}\right) dx'\, dy' = \frac{-ab}{Z_w} C(r_0,\phi_0,z_0) \quad (10)$$

where a is the width of the waveguide feeder, b is its height, and Z_w is the wave impedance. The factor $C(r_0,\phi_0,z_0)$ represents the amplitude of the electric field induced in the probe waveguide when only generator A is activated. It is a function of the position of the probe antenna with respect to the test antenna. The integral has been normalized by the amplitude of the electric field in the waveguide when generator B alone is activated. If generator B is replaced by a matched linear detector when only generator A is activated, the detector output voltage will be proportional to $C(r_0,\phi_0,z_0)$. Thus the expression for I_4 can be written

$$I_4 = -K \frac{ab}{Z_w} v(r_0,\phi_0,z_0) \quad (11)$$

where K is a constant of proportionality and $v(r_0,\phi_0,z_0)$ is the detector output voltage.

To evaluate the integral for I_1 in (9), the cylindrical wave expansions of the fields over Σ_1 will be written initially in the forms

$$\boldsymbol{E}_a(r) = a_n(h)\boldsymbol{M}_{nh}^4(r) + b_n(h)\boldsymbol{N}_{nh}^4(r) \tag{12}$$

$$\boldsymbol{H}_a(r) = \frac{-k}{j\omega\mu}\left(b_n(h)\boldsymbol{M}_{nh}^4(r) + a_n(h)\boldsymbol{N}_{nh}^4(r)\right) \tag{13}$$

$$\boldsymbol{E}_b(r') = c_m(\eta)\boldsymbol{M}_{m\eta}^4(r') + d_m(\eta)\boldsymbol{N}_{m\eta}^4(r') \tag{14}$$

$$\boldsymbol{H}_b(r') = \frac{-k}{j\omega\mu}\left(d_m(\eta)\boldsymbol{M}_{m\eta}^4(r') + c_m(\eta)\boldsymbol{N}_{m\eta}^4(r')\right). \tag{15}$$

After I_1 is evaluated for these fields, the result must be summed in m and n and integrated in η and h to obtain the final value of the integral.

With the vector translation theorems developed in Appendix A, the origin for $\boldsymbol{E}_b$ and $\boldsymbol{H}_b$ is first changed from 0′ to 0. The result is

$$\boldsymbol{E}_b(r) = \sum_{l=-\infty}^{\infty}(-1)^l H_{m+l}^{(2)}(\lambda r_0)\exp(jl\phi_0)\exp(j\eta z_0)\cdot\left(c_m(\eta)\boldsymbol{M}_{-l\eta}^1(r) + d_m(\eta)\boldsymbol{N}_{-l\eta}^1(r)\right) \tag{16}$$

$$\boldsymbol{H}_b(r) = \frac{-k}{j\omega\mu}\sum_{l=-\infty}^{\infty}(-1)^l H_{m+l}^{(2)}(\lambda r_0)\exp(jl\phi_0)\exp(j\eta z_0)\cdot\left(d_m(\eta)\boldsymbol{M}_{-l\eta}^1(r) + c_m(\eta)\boldsymbol{N}_{-l\eta}^1(r)\right) \tag{17}$$

where $\lambda = (k^2 - \eta^2)^{1/2}$. Substitution of these expressions and those for $\boldsymbol{E}_a$ and $\boldsymbol{H}_a$ into the integrand for I_1 gives

$$\begin{aligned} I_1 = \frac{k}{j\omega\mu}\sum_{l=-\infty}^{\infty}(-1)^l H_{m+l}^{(2)}(\lambda r_0)\exp(jl\phi_0) \\ \cdot\exp(j\eta z_0)\int_{-\infty}^{\infty}\int_{-\pi}^{\pi}\left((a_n(h)d_m(\eta) + b_n(h)c_m(\eta))\right. \\ \cdot(\boldsymbol{M}_{nh}^4 \times \boldsymbol{M}_{-l\eta}^1 + \boldsymbol{N}_{nh}^4 \times \boldsymbol{N}_{-l\eta}^1) \\ + (a_n(h)c_m(\eta) + b_n(h)d_m(\eta)) \\ \left.\times(\boldsymbol{M}_{nh}^4 \times \boldsymbol{N}_{-l\eta}^1 + \boldsymbol{N}_{nh}^4 \times \boldsymbol{M}_{-l\eta}^1)\right)\cdot\hat{r}r_1\,d\phi\,dz \end{aligned} \tag{18}$$

where the vectors $\boldsymbol{M}$ and $\boldsymbol{N}$ are functions of the (r,ϕ,z).

From the orthogonality properties of the cylindrical wave vectors developed in Appendix B, it follows that the terms involving the products $\boldsymbol{M}_{nh}^4 \times \boldsymbol{M}_{-l\eta}^1\cdot\hat{r}$ and $\boldsymbol{N}_{nh}^4 \times \boldsymbol{N}_{-l\eta}^1\cdot\hat{r}$ have zero contribution to (18). The remaining terms can be evaluated with the aid of (B3). Thus I_1 becomes

$$\begin{aligned} I_1 = \frac{kr_1}{j\omega\mu}\sum_{l=-\infty}^{\infty}(-1)^l H_{m+l}^{(2)}(\lambda r_0)\exp(jl\phi_0)\exp(j\eta z_0) \\ \cdot(a_n(h)c_m(\eta) + b_n(h)d_m(\eta))\left(\frac{4\pi^2\Lambda^3}{k}\delta_{nl}\delta(\eta + h)\right. \\ \left.\cdot(J_{-n}'(\Lambda r_1)H_n^{(2)}(\Lambda r_1) - J_{-n}(\Lambda r_1)H_n^{(2)\prime}(\Lambda r_1))\right) \end{aligned} \tag{19}$$

where δ_{nl} is the Kronecker delta and $\delta(\eta + h)$ is the Dirac delta function. This expression can be simplified with the aid of the identity

$$J_{-n}'(\Lambda r_1)H_n^{(2)}(\Lambda r_1) - J_{-n}(\Lambda r_1)H_n^{(2)\prime}(\Lambda r_1) = \frac{j2(-1)^n}{\pi\Lambda r_1} \tag{20}$$

Thus I_1 reduces to

$$\begin{aligned} I_1 = \frac{8\pi\Lambda^2}{\omega\mu}H_{n+m}^{(2)}(\Lambda r_0)\exp(jn\phi_0)\exp(j\eta z_0)\delta(\eta + h) \\ \cdot(a_n(h)c_m(\eta) + b_n(h)d_m(\eta)) \end{aligned} \tag{21}$$

which is independent of r_1. When this expression is summed over all m and n and integrated in η and h, the result is

$$\begin{aligned} I_1 = \frac{8\pi\Lambda^2}{\omega\mu}\sum_{n=-\infty}^{\infty}\exp(jn\phi_0)\int_{-\infty}^{\infty}\left(a_n(h)\sum_{m=-\infty}^{\infty}c_m(-h)\right. \\ \cdot H_{n+m}^{(2)}(\Lambda r_0) + b_n(h)\sum_{m=-\infty}^{\infty}d_m(-h)H_{n+m}^{(2)}(\Lambda r_0)) \\ \left.\cdot\exp(-jhz_0)\,dh\right. \end{aligned} \tag{22}$$

Since multiple scattering is neglected, $\boldsymbol{E}_a$, $\boldsymbol{H}_a$, $\boldsymbol{E}_{as}$, and $\boldsymbol{H}_{as}$ satisfy the homogeneous wave equation outside of Σ_a. Thus by the Lorentz reciprocity theorem it follows that I_2 is identically zero. Similarly, I_3 is also zero. Thus it follows that (9) reduces to

$$\begin{aligned} v(r_0,\phi_0,z_0) = \frac{\Lambda^2}{4\pi^2k^2}\sum_{n=-\infty}^{\infty} \\ \cdot\exp(jn\phi_0)\int_{-\infty}^{\infty}\left(a_n(h)\sum_{m=-\infty}^{\infty}c_m(-h)\right. \\ \left.\cdot H_{n+m}^{(2)}(\Lambda r_0) + b_n(h)\sum_{m=-\infty}^{\infty}d_m(-h)\right. \\ \left.\cdot H_{n+m}^{(2)}(\Lambda r_0))\exp(-jhz_0)\,dh\right. \end{aligned} \tag{23}$$

where $v(r_0,\phi_0,z_0)$ has been normalized by choosing the constant of proportionality in (11) to be $32\pi^3Z_wk^2/\omega\mu ab$.

Examination of this equation reveals that $v(r_0,\phi_0,z_0)$ is in the form of a Fourier series in ϕ_0 and a Fourier integral in z_0. Thus the equation has an inverse which is given by

$$\begin{aligned} a_n(h)\sum_{m=-\infty}^{\infty}c_m(-h)H_{n+m}^{(2)}(\Lambda r_0) \\ + b_n(h)\sum_{m=-\infty}^{\infty}d_m(-h)H_{n+m}^{(2)}(\Lambda r_0) \\ = \frac{k^2}{\Lambda^2}\int_{-\infty}^{\infty}\int_{-\pi}^{\pi}v(r_0,\phi_0,z_0)\exp(-jn\phi_0)\exp(jhz_0)\,d\phi_0\,dz_0. \end{aligned} \tag{24}$$

This is the desired result. It relates the cylindrical wave amplitude weighting functions $a_n(h)$ and $b_n(h)$ of an arbitrary test antenna to the two-dimensional Fourier transform of the output voltage of a probe antenna when the measurement surface is a cylinder of radius r_0. If the cylindrical wave amplitude weighting functions for the probe antenna are known, it follows that (24) can be solved for $a_n(h)$ and $b_n(h)$ provided two independent measurements of $v(r_0,\phi_0,z_0)$ are made.

Let $v'(r_0,\phi_0,z_0)$ represent the voltage output of the probe antenna when it is rotated 90° about its longitudinal axis. An equation identical to (24) can be written which relates $a_n(h)$ and $b_n(h)$ to $v'(r_0,\phi_0,z_0)$ with the exception that $c_m(-h)$ and $d_m(-h)$ must be replaced by the amplitude weighting functions for the rotated probe. If these are denoted by $c_m'(-h)$ and $d_m'(-h)$, then this equation and (24) can be solved simultaneously for $a_n(h)$ and $b_n(h)$ to obtain

$$a_n(h) = \frac{k^2}{\Lambda^2\Delta_n(h)} \left(I_n(h) \sum_{m=-\infty}^{\infty} d_m'(-h)H_{n+m}^{(2)}(\Lambda r_0) - I_n'(h) \sum_{m=-\infty}^{\infty} d_m(-h)H_{n+m}^{(2)}(\Lambda r_0)\right) \quad (25)$$

$$b_n(h) = \frac{k^2}{\Lambda^2\Delta_n(h)} \left(I_n'(h) \sum_{m=-\infty}^{\infty} c_m(-h)H_{n+m}^{(2)}(\Lambda r_0) - I_n(h) \sum_{m=-\infty}^{\infty} c_m'(-h)H_{n+m}^{(2)}(\Lambda r_0)\right) \quad (26)$$

where

$$I_n(h) = \int_{-\infty}^{\infty}\int_{-\pi}^{\pi} v(r_0,\phi_0,z_0) \exp(-jn\phi_0) \exp(jhz_0)\, d\phi_0\, dz_0 \quad (27)$$

$$I_n'(h) = \int_{-\infty}^{\infty}\int_{-\pi}^{\pi} v'(r_0,\phi_0,z_0) \exp(-jn\phi_0) \exp(jhz_0)\, d\phi_0\, dz_0 \quad (28)$$

$$\Delta_n(h) = \left(\sum_{m=-\infty}^{\infty} c_m(-h)H_{n+m}^{(2)}(\Lambda r_0)\right) \cdot \left(\sum_{m=-\infty}^{\infty} d_m'(-h)H_{n+m}^{(2)}(\Lambda r_0)\right) - \left(\sum_{m=-\infty}^{\infty} c_m'(-h)H_{n+m}^{(2)}(\Lambda r_0)\right) \cdot \left(\sum_{m=-\infty}^{\infty} d_m(-h)H_{n+m}^{(2)}(\Lambda r_0)\right). \quad (29)$$

It is assumed that the probe responds predominantly to one polarization component so that a solution for $a_n(h)$ and $b_n(h)$ exists, i.e., $\Delta_n(h)$ must not be zero.

Equations (25) through (29) form the basis of the method for the determination of the far field of an arbitrary antenna from measurements made with a probe on a cylinder containing the antenna. By using these equations to determine the cylindrical wave amplitude weighting functions $a_n(h)$ and $b_n(h)$, the far field of the antenna can be determined from (6) and (7). Since the far field is determined from only those values of $a_n(h)$ and $b_n(h)$ for which $-k \leq h \leq k$, it follows that the cylindrical wave amplitude weighting functions of the probe need be known only for arguments inside this interval.

IV. Numerical Considerations

A. Method of Evaluating Far Field from Measured Data

It has been shown that, over the surface of a sphere of radius R, the far-field electric field intensity radiated by an antenna can be written in the form

$$E_\theta(\theta,\phi) = j \sin\theta \sum_{n=-\infty}^{\infty} j^n b_n(k\cos\theta) \exp(jn\phi) \quad (30)$$

$$E_\phi(\theta,\phi) = \sin\theta \sum_{n=-\infty}^{\infty} j^n a_n(k\cos\theta) \exp(jn\phi) \quad (31)$$

where the constant factor $-2k \exp(-jkR)/R$ has been suppressed in each equation. In these equations $a_n(h)$ and $b_n(h)$, where $h = k\cos\theta$, are the amplitude weighting functions of the cylindrical wave vectors $\boldsymbol{M}$ and $\boldsymbol{N}$, respectively, in the cylindrical wave expansion of the field radiated by the antenna. In this section a numerical solution for $a_n(h)$ and $b_n(h)$ is developed which is based on the results of the previous section. The numerical evaluation of (30) and (31) for the far field of the antenna is then described.

Let the measurement cylinder be divided into a lattice of points with coordinates $(r_0,n\Delta\phi,m\Delta z)$ where $0 \leq n \leq N-1$, $0 \leq m \leq M-1$, and M and N are positive integers. To exactly evaluate (27) and (28) from the output voltages of the probe at these points, two conditions must be satisfied. First, v and v' must be zero when $z < 0$ and $z > (M-1)\Delta z$. Second, v and v' must have no angular harmonic n greater than $\pi/\Delta\phi$ and must be wavenumber limited in h to a maximum wavenumber less than or equal to $\pi/\Delta z$. The first condition cannot be met with any radiating structure. However, if the test antenna is aligned in the cylinder so that it does not radiate appreciably in the $\pm z$ direction, it can be met approximately if M is chosen large enough. The second condition can be met if the sample intervals $\Delta\phi$ and Δz are not too large.

Since high-Q antennas are rarely encountered in practice, practical upper bounds on $\Delta\phi$ and Δz can be obtained by studying the antenna Q. Collin and Rothschild [11] have evaluated the Q of single modes in the cylindrical wave expansion of a radiating structure as a function of the mode indices n and h. From their work, it follows that the Q of an antenna can become large if there is any significant energy in cylindrical waves for

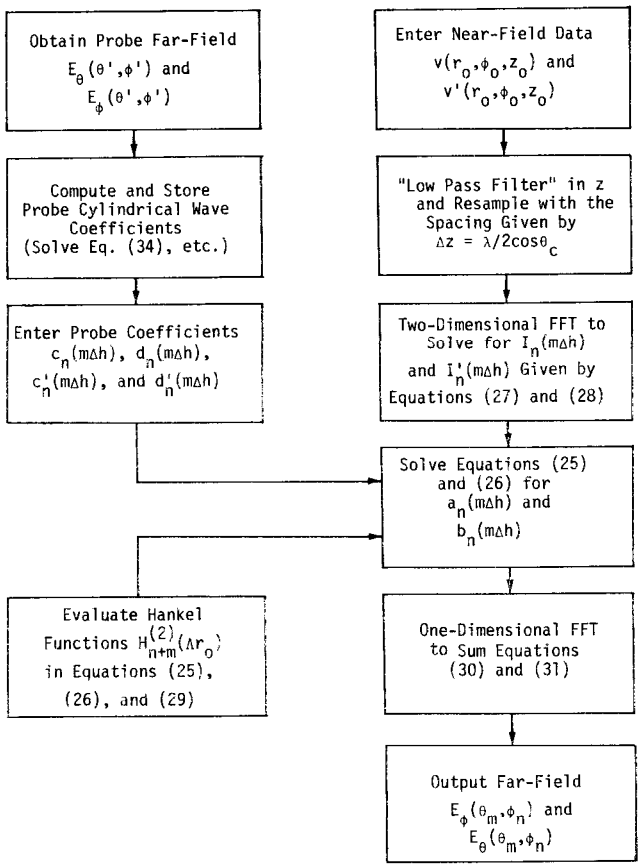

Fig. 3. Flow-diagram for far-field evaluation.

which $h > k$ or $n > ka$, where a is the radius of the smallest cylinder with center coinciding with the z axis and which completely encloses the antenna. Thus it follows that practical upper bounds on the sample intervals are $\Delta\phi = \pi/ka$ and $\Delta z = \lambda/2$.

Assuming that the preceding conditions are met, the integrals for $I_n(h)$ and $I_n'(h)$ can be evaluated easily with a two-dimensional fast Fourier transform (FFT) algorithm. The FFT is an extremely efficient algorithm for the evaluation of the Fourier integral. When used to evaluate (27) and (28), the integrals for $I_n(h)$ and $I_n'(h)$ are evaluated for all ordered pairs (n,h) such that $-N/2 \leq n \leq N/2 - 1$ and $h = m\Delta h$, where $\Delta h = 2\pi/M\Delta z$ and $-M/2 \leq m \leq M/2 - 1$. Since the far-field expressions for $E_\theta(\theta,\phi)$ and $E_\phi(\theta,\phi)$ are evaluated at $h = k\cos\theta$, the values of θ corresponding to $h = m\Delta h$ are given by $\theta_m = \cos^{-1}(m\lambda/M\Delta z)$.

Inasmuch as it is impossible to measure the near field over a complete cylinder enclosing an antenna, the present method for determining the far field of the test antenna is most suitable when applied to antennas which radiate predominantly in the annular region about $\theta = \pi/2$ defined by $\theta_c < \theta \leq \pi - \theta_c$. In order for all θ_m defined earlier to lie in this interval, it follows that Δz must satisfy $\Delta z = \lambda/2\cos\theta_c$. However, for $\theta_c \neq 0$ this condition violates the z-sample spacing criterion of $\Delta z \leq \lambda/2$.

This problem can be overcome by "low-pass filtering" the near-field data in z and then resampling at the rate given in the preceding. This can be accomplished easily with the FFT. First, the near-field data arrays are transformed in z so that on output the wavenumber spacing is $\Delta h = 2\pi/M\Delta z$. Second, only the elements in the transformed arrays corresponding to values of m such that $|m| \leq M\Delta z\cos\theta_c/\lambda$ are inverse transformed to create the filtered arrays with M' elements in z where $M' < M$. It follows that the z-sample spacing in these arrays is given by $\Delta z = \lambda/2\cos\theta_c$. Finally, the filtered arrays are augmented with $M - M'$ zeros so that the final arrays again contain M elements in z. It can be shown that when these arrays are transformed with the FFT, all M values of θ_m defined earlier lie in the desired interval $\theta_c < \theta_m \leq \pi - \theta_c$.

After the evaluation of $I_n(m\Delta h)$ and $I_n'(m\Delta h)$, the cylindrical wave amplitude weighting functions $a_n(m\Delta h)$ and $b_n(m\Delta h)$ can be solved for using (25) and (26). (The evaluation of the coefficients in these equations which are determined by the probe will be discussed under the following heading.) The calculation of the far-field electric field intensity radiated by the test antenna can be achieved then by performing the summations indicated in (30) and (31). Again, this can be done most efficiently with the FFT algorithm. However, each $a_n(m\Delta h)$ and $b_n(m\Delta h)$ must be multiplied by the factors $j^n\sin\theta_m$ and $j^{n+1}\sin\theta_m$, respectively, before the FFT can be used to perform the summations. The far-field components so computed will be $E_\theta(\theta_m,\phi_n)$ and $E_\phi(\theta_m,\phi_n)$, where

$$\phi_n = \frac{2n\pi}{N}, \qquad 0 \leq n \leq N-1 \tag{32}$$

$$\theta_m = \cos^{-1}\left[\frac{m\cos\theta_c}{(M/2)}\right], \qquad -\frac{M}{2} \leq m \leq \frac{M}{2} - 1. \tag{33}$$

The preceding operations are summarized in the flow diagram of Fig. 3. In the digital computer implementation of these computations, the majority of the calculations can be performed "in-place" so that the input near-field data arrays are finally replaced by the output far-field values. This leads to a more efficient use of computer space.

B. Probe Coefficients

To evaluate (25) and (26) for the amplitude weighting functions in the cylindrical wave expansion of the far field radiated by the test antenna, it is necessary to know the amplitude weighting functions in the expansion of the field radiated by the probe. Since it is necessary to known these functions only for the wavenumbers h such that $|h| \leq k$, it is possible to obtain them from a knowledge of the far field radiated by the probe when it is connected to a signal source. Two near-field probes were used in the experimental phase of the research, one an open-end WR-90 waveguide and the other a WR-90 waveguide terminating in a pyramidal horn with a 5.7° E-plane half-angle flare and a 15.7° H-plane half-angle flare. The aperture dimensions of the two probes were

1 in × 0.5 in and 1.88 in × 0.81 in, respectively. The two probes had been calibrated at 9.68 GHz for use with the near-field range at Georgia Institute of Technology [3]. The calibration data consisted of the measured amplitude and phase of the far-field components $E_\theta(\theta,\phi)$ and $E_\phi(\theta,\phi)$ of the probes over a sector of a sphere defined by $30° \leq \theta \leq 150°$ and $-60° \leq \phi \leq 60°$. The step sizes in the far-field data were $\Delta\theta = 5°$ and $\Delta\phi = 1°$.

Since it is necessary to resolve the measured probe data into Fourier series in the azimuth angle ϕ, some upper limit on the maximum angular harmonic for each probe must be established. This can be done by using the criterion established by Harrington [10] that the maximum significant angular harmonic is $N = ka$, where a is the radius of the smallest sphere completely enclosing the aperture of the probe. At 9.68 GHz, it follows that the smallest integer greater than ka for each probe is $N = 3$ for the open-end waveguide and $N = 6$ for the small horn.

Let the probe antenna be oriented as shown in Fig. 4. Aside from the factor $-2k \exp(-jkR)/R$, the far-field electric field intensity radiated by the probe can be expressed by (30) and (31) with $b_n(h)$ and $a_n(h)$ replaced by $d_n(h)$ and $c_n(h)$, respectively, with $h = k \cos\theta$. If the probe is rotated 90° in the right-hand sense about the x axis, the far-field components $E_\theta'(\theta,\phi)$ and $E_\phi'(\theta,\phi)$ can be expressed similarly using the cylindrical wave weighting functions $d_n'(h)$ and $c_n'(h)$. In order to compensate for the effects of the probe in calculating the far field of the test antenna, it is necessary to know $c_n(h)$, $d_n(h)$, $c_n'(h)$, and $d_n'(h)$ with the argument $h = -k \cos\theta_m = k \cos(180° - \theta_m)$, where θ_m is the elevation angle at which the far field of the test antenna is to be computed.

Since the far-field components radiated by the probe are in the form of a Fourier series in ϕ, the amplitude weighting functions for a particular value of θ can be obtained by numerically evaluating the Fourier inversion integral from the measured fields. However, an alternate procedure was used in this research since the far field of the probe was known only for $-60° \leq \phi \leq 60°$. The approach taken was to perform a least squares curve fit of the far-field expressions to the measured probe data.

For example, it can be shown that the expression for $E_\theta(\theta,\phi)$ approximates the measured $E_\theta(\theta,\phi)$ in the least squares senses sense if the $d_n(k \cos\theta)$ satisfy the system of equations

$$\sum_{n=-N}^{N} d_n(k\cos\theta)\frac{\sin(m-n)\phi_1}{(m-n)\phi_1} = \frac{1}{2j^{m+1}\sin\theta}\int_{-\phi_1}^{\phi_1} E_\theta(\theta,\phi) \cdot \exp(-jm\phi)\,d\phi \quad (34)$$

where $-N \leq m \leq N$. The $d_n(k \cos\theta)$ for the test probes were obtained by solving this system of equations with the Gauss–Jordan method for solving simultaneous equations. The integral on the right of (34) was evaluated from the measured data by using the trapezoidal rule for numerical integration with a step size of 1° and

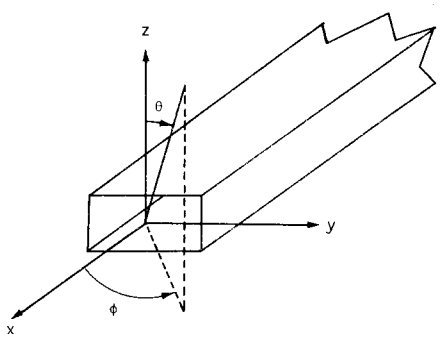

Fig. 4. Coordinate system for probe antenna.

$\phi_1 = 60°$. The solutions for $d_n(k \cos\theta)$ were obtained for $-N \leq n \leq N$ and $30° \leq \theta \leq 150°$ with a step size in θ of 5°. Solutions for $c_n(k \cos\theta)$, $d_n'(k \cos\theta)$, and $c_n'(k \cos\theta)$ were obtained for each probe in a similar way. In the case of the rotated probe, the far-field $E_\theta'(\theta,\phi)$ and $E_\phi'(\theta,\phi)$ were obtained from the measured $E_\theta(\theta,\phi)$ and $E_\phi(\theta,\phi)$ using numerical interpolation and the necessary coordinate transformations.

V. Experimental Results

A. Test Antenna

The experimental work was implemented to verify the theory and to demonstrate the practicality of calculating the far-field pattern of an antenna from near-field measurements on a cylinder. The test antenna was a ten-element resonant array of longitudinal shunt slots cut into the broad wall of a section of WR-90 waveguide. The slots were designed so that the antenna radiated a Chebyschev pattern with sidelobe levels of −20 dB. The load end of the waveguide array was terminated in an adjustable short which was set for minimum input VSWR at the measurement frequency of 9.68 GHz.

B. Near-Field Measurements

The near-field measurement system consisted of a rotating platform on which the test antenna was mounted and a probe positioning mechanism capable of positioning the probe to any point on a 100-in vertical line parallel to the axis of rotation of the platform. The probe mechanism was aligned so that the longitudinal axis of the probe intersected the axis of rotation of the platform one foot from the mouth of the probe. The rotating platform and the probe mechanism were servo-controlled and could be positioned remotely.

The near-field data $v(r_0,\phi_0,z_0)$ and $v'(r_0,\phi_0,z_0)$ were measured separately over the cylinder by rotating the antenna platform and moving the probe vertically. To minimize amplitude and phase errors in the signal path due to the motion of the antenna platform and the probe mechanism, rotary signal joints were incorporated at all axes of rotation. The near-field amplitude and phase data were recorded on an FM tape deck and subsequently transferred to a digital computer via an analog-to-digital converter.

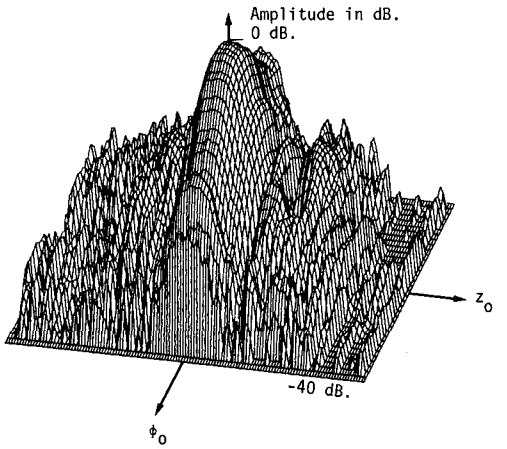

(a)

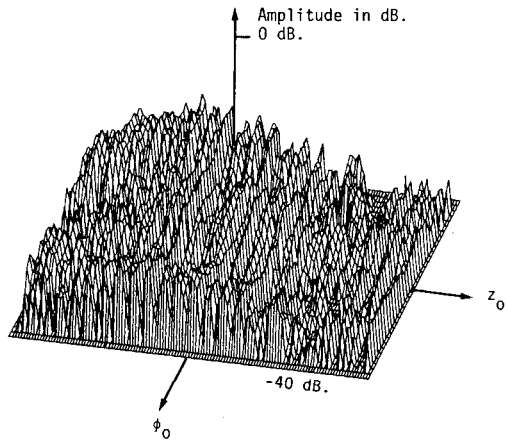

(b)

Fig. 5. Near-field amplitude and phase patterns for measurement case one. (a) Amplitude and phase patterns of E_ϕ. (b) Amplitude and phase patterns of E_θ.

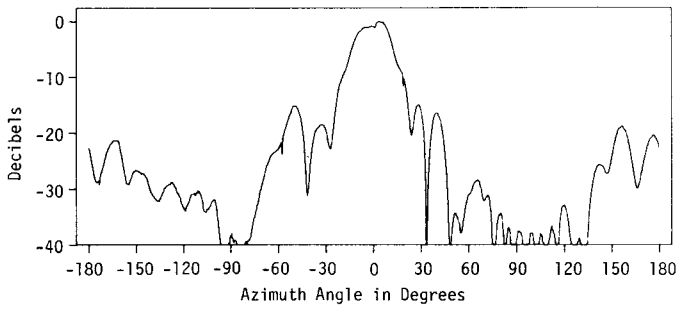

(a)

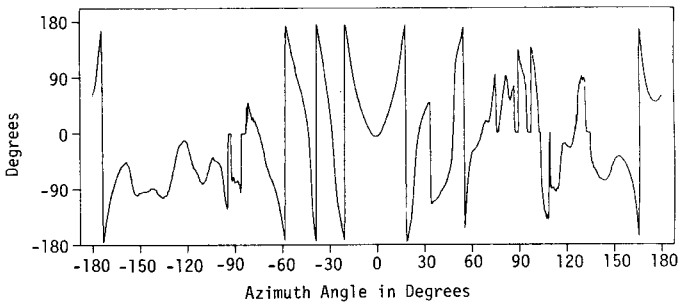

(b)

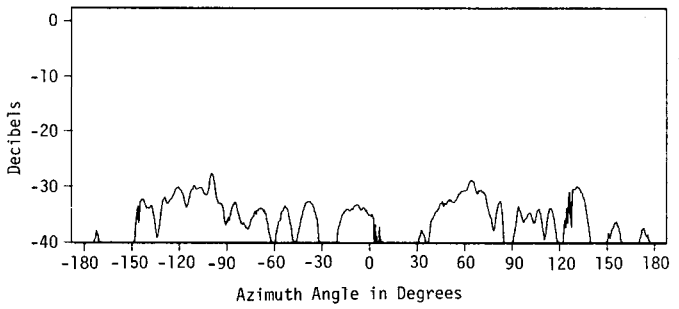

(c)

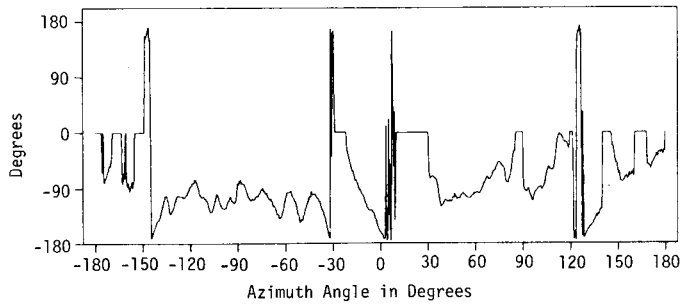

(d)

Fig. 6. Near-field amplitude and phase patterns for measurement case two. (a) Amplitude of E_θ. (b) Phase of E_θ. (c) Amplitude of E_ϕ. (d) Phase of E_ϕ.

To minimize reflections and stray radiation, the nearest reflecting surfaces in the vicinity of the near-field range and the klystron signal source and its associated hardware were covered with a limited supply of absorbing material. It is estimated that the repeatability of the measurements was ± 0.5 dB in amplitude and $\pm 3°$ in phase. The dynamic range of the measurement system was 40 dB.

The measured near-field amplitude and phase patterns of the test antenna are shown in Figs. 5 and 6. In Fig. 5,

the antenna was centered vertically in the measurement cylinder. The near field in this case was sampled at intervals on the cylinder of $\Delta\phi = 11.25°$ and $\Delta z = \lambda/3$. The height of the cylinder was 52.1 in or 128 one-third wavelengths at 9.68 GHz. In Fig. 6, the antenna was centered horizontally in the measurement cylinder. The near-field elevation pattern was so broad in this case that the field was measured only on a circle around the antenna. The near field in this case was sampled 1024 times in the azimuth angle ϕ.

C. Calculated Far-Field Patterns

The calculation of the far-field patterns was performed on a Univac 1108 digital computer. The input data consisted of the measured near-field components of the test antenna and the cylindrical wave amplitude weighting functions for the probe. The computational process has been described in Section IV.

The three-dimensional far-field amplitude pattern of E_ϕ which was calculated from the measurement with the antenna mounted vertically in the cylinder is displayed in Fig. 7. The base coordinates in this figure are the azimuth angle ϕ, where $-180° \leq \phi \leq 180°$, and the wavenumber $h = k \cos\theta$, where $30° < \theta \leq 150°$. Although the cross polarization pattern was calculated, it was too low in amplitude to be interpreted meaningfully. In Fig. 8, the principal plane amplitude patterns representing the two cuts $\phi = 0°$ and $\theta = 90°$ in Fig. 7 are displayed with the measured relative far-field patterns of the test antenna. There is strong evidence that the discrepancies between the measured and calculated patterns in this figure were caused by reflections from unshielded objects in the vicinity of the near-field range. A limited supply of RF absorber made it impossible to cover all reflecting objects over the full 360° circle illuminated by the test antenna as it rotated on the rotating platform.

Fig. 9 displays the calculated far-field azimuth pattern of E_θ for the measurement case with the antenna mounted horizontally. Again the cross polarization pattern has been omitted.

For the sake of brevity, only two measurement cases have been discussed here. In this research, however, the near field of the test antenna was measured for four different cases corresponding to three orientations of the test antenna in the measurement cylinder and to two different near-field probes. The omitted measurements and calculations for the other cases are in full agreement with the results presented here.

VI. Conclusion

It has been shown and experimentally verified that it is possible to calculate the far-field pattern of an antenna from measurements on a cylinder with a probe with arbitrary, but known characteristics. In addition, it has been demonstrated that the necessary calculations can be implemented on the digital computer with the FFT algorithm. The equipment necessary to experimentally implement the near-field measurements is a rotating

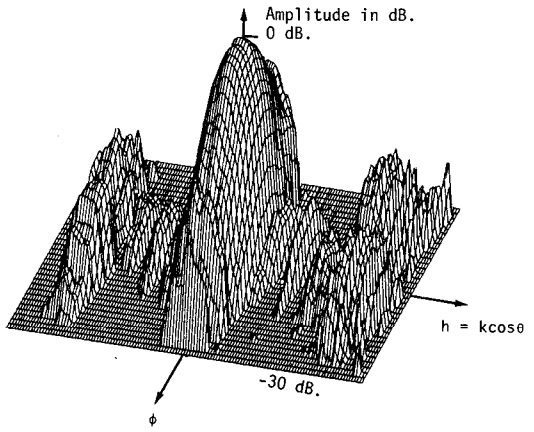

Fig. 7. Calculated far-field amplitude pattern of E_ϕ for measurement case one.

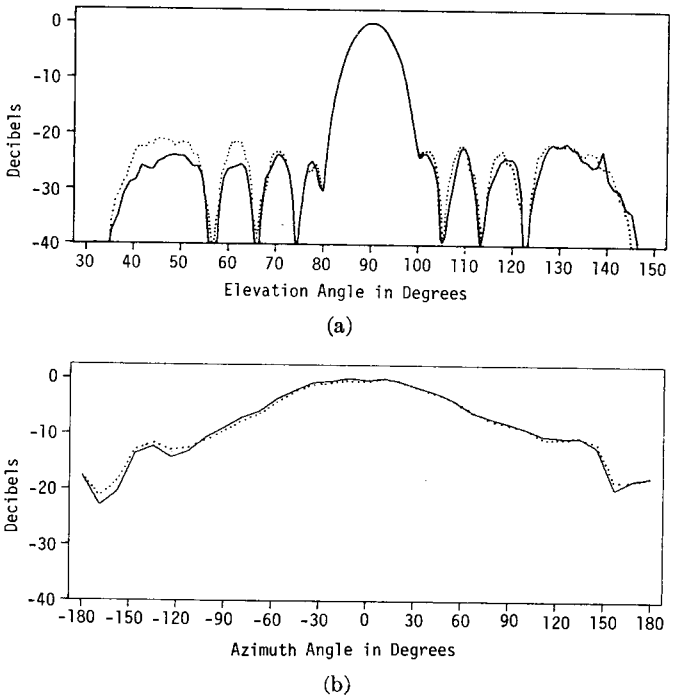

Fig. 8. Comparison of principal plane amplitude patterns calculated for measurement case one (———) to measured amplitude patterns (••••••).

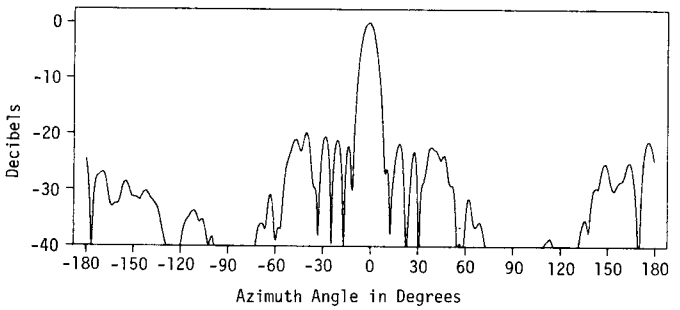

Fig. 9. Calculated far-field amplitude pattern of E_θ for measurement case two.

platform on which the test antenna is mounted, a linear motion mechanism to move the probe in a vertical line up the measurement cylinder, and the necessary signal detection and recording system.

It may seem that probe compensation is not a significant consideration when the near-field measurement surface is a cylinder. As far as the azimuth pattern of the test antenna at a fixed elevation angle is concerned, this is true if one is not interested in precision measurements since the probe is always pointed toward the center of the measurement cylinder. However, probe correction is an important consideration in calculating the elevation pattern of the test antenna. This follows since the elevation pattern is predominantly determined by the axial variation of the near-field data on the cylinder. In any case, there is essentially no difference in the numerical work necessary to calculate the far-field patterns with or without probe compensation [9]. Once the probe coefficients have been determined, the only difference between the two cases is the Hankel functions which enter the solution. Without probe compensation, both these functions and their first derivatives must be evaluated, while derivatives of the Hankel functions do not enter the probe compensated solution.

Compared to the plane wave approach for which the far-field pattern can be calculated for only one hemisphere of space without repeating the procedure, the method which has been described here is advantageous when applied to antennas for which it is desired to calculate the complete 360° far-field azimuth pattern. It is limited to far-field elevation angles which do not include 0° and 180° since the Hankel functions in the cylindrical wave expansions are not defined for these angles. In cases where the antenna radiates a broad, but symmetrical elevation pattern, it has been experimentally demonstrated that the broadside azimuth pattern can be calculated from near-field measurements on a circle around the antenna. This can be particularly advantageous in the case of large microwave antennas which might require the accumulation of a prohibitively large amount of data to compute a two-dimensional far-field pattern.

Appendix A

Vector Translation Theorems for Cylindrical Vector Wave Functions

Let the coordinates (r_0,ϕ_0,z_0) be the location of the origin of the coordinate system (r',ϕ',z') in the coordinate system (r,ϕ,z) as shown in Fig. 10. It is desired to express the cylindrical vector wave functions $\boldsymbol{M}_{nh}^4(r')$ and $\boldsymbol{N}_{nh}^4(r')$ as functions of the coordinates (r,ϕ,z).

In the system $(r'\phi',z')$ the generating function ψ_{nh}^4 for these vectors is given by

$$\psi_{nh}^4(r') = H_n^{(2)}(\Lambda r') \exp(jn\phi') \exp(-jhz'). \quad \text{(A1)}$$

This can be expressed as a function of (r,ϕ,z) by using Graf's addition theorem for the Hankel function, which states

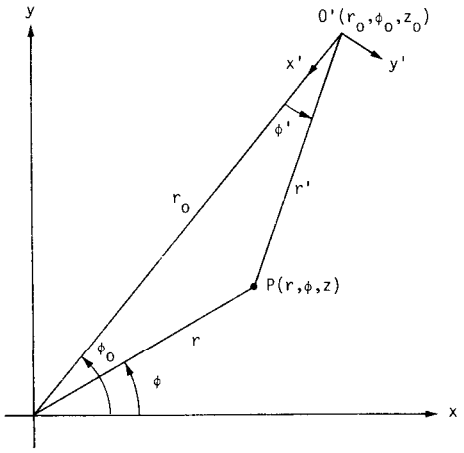

Fig. 10. Coordinate system for cylindrical wave translation theorems.

$$H_n^{(2)}(\Lambda r') = \exp(-jn\phi') \sum_{m=-\infty}^{\infty} H_{n+m}^{(2)}(\Lambda r_0) J_m(\Lambda r) \cdot \exp[jm(\phi - \phi_0)]. \quad \text{(A2)}$$

When this is substituted into (A1), the generating function is transformed into

$$\psi_{nh}^4(r') = \sum_{m=-\infty}^{\infty} (H_{n+m}^{(2)}(\Lambda r_0) \exp(jm\phi_0) \exp(jhz_0)) \cdot J_m(\Lambda r) \exp(-jm\phi) \exp(-jhz). \quad \text{(A3)}$$

The vectors $\boldsymbol{M}_{nh}^4$ and $\boldsymbol{N}_{nh}^4$ are obtained by the following operations on ψ_{nh}^4:

$$\boldsymbol{M}_{nh}^4 = \nabla' \times \hat{z}\psi_{nh}^4 \quad \text{(A4)}$$

$$\boldsymbol{N}_{nh}^4 = \frac{1}{k} \nabla' \times \boldsymbol{M}_{nh}^4 \quad \text{(A5)}$$

where the primes denote operations on the primed coordinates (r',ϕ',z'). Since the del operator is invariant to a coordinate transformation, these become

$$\boldsymbol{M}_{nh}^4(r') = \sum_{m=-\infty}^{\infty} (H_{n+m}^{(2)}(\Lambda r_0) \exp(jm\phi_0) \exp(jhz_0) \cdot \nabla \times (\hat{z}J_m(\Lambda r) \exp(-jm\phi) \exp(-jhz)) \quad \text{(A6)}$$

$$\boldsymbol{N}_{nh}^4(r') = \frac{1}{k} \sum_{m=-\infty}^{\infty} (H_{n+m}^{(2)}(\Lambda r_0) \exp(jm\phi_0) \exp(jhz_0)) \cdot \nabla \times \nabla \times (\hat{z}J_m(\Lambda r) \exp(-jm\phi) \exp(-jhz)) \quad \text{(A7)}$$

From the definitions

$$\boldsymbol{M}_{nh}^1 = \nabla \times (\hat{z}J_m(\Lambda r) \exp(-jm\phi) \exp(-jhz)) = \nabla \times \hat{z}\psi_{nh}^1 \quad \text{(A8)}$$

$$\boldsymbol{N}_{nh}^1 = \frac{1}{k} \nabla \times \boldsymbol{M}_{nh}^1(r) \quad \text{(A9)}$$

it follows that (A6) and (A7) reduce to

$$\boldsymbol{M}_{nh}^4(r') = \sum_{m=-\infty}^{\infty} (-1)^m H_{n+m}^{(2)}(\Lambda r_0) \exp(jm\phi_0) \cdot \exp(jhz_0) \boldsymbol{M}_{-mh}^1(r) \quad \text{(A10)}$$

$$N_{nh}{}^4(r') = \sum_{m=-\infty}^{\infty} (-1)^m H_{n+m}{}^{(2)}(\Lambda r_0) \exp(jm\phi_0) \cdot \exp(jhz_0) N_{-mn}{}^1(r). \quad \text{(A11)}$$

These are the desired translation theorems. They are valid for all $r \leq r_0$.

Appendix B

Orthogonality Properties of Cylindrical Wave Vectors

Property A

$$\int_{-\infty}^{\infty}\int_{-\pi}^{\pi} \boldsymbol{M}_{nh}{}^i \times \boldsymbol{M}_m{}^i \cdot \hat{r}\, d\phi\, dz = 0, \quad \forall\, m, n, \eta, \text{ and } h. \quad \text{(B1)}$$

This property follows from the fact that the vector $\boldsymbol{M}$ contains no z component. Thus the product $\boldsymbol{M}_{nh}{}^i \times \boldsymbol{M}_{m\eta}{}^j$ has only a z component which is zero when scalar multiplied by the unit vector $\hat{r}$.

Property B

$$\int_{-\infty}^{\infty}\int_{-\pi}^{\pi} N_{nh}{}^i \times N_m{}^i \cdot \hat{r}\, d\phi\, dz = 0, \quad \forall\, m, n, \eta, \text{ and } h. \quad \text{(B2)}$$

The integrand in (B2) can be simplified as follows:

$$N_{nh}{}^i \times N_{m\eta}{}^j \cdot \hat{r} = N_{m\eta}{}^j \cdot (\hat{r} \times N_{nh}{}^i) = \left(\frac{nh\lambda^2}{k^2 r} Z_n{}^i(\Lambda r) Z_m{}^i(\lambda r) - \frac{m\eta\Lambda^2}{k^2} Z_n{}^i(\Lambda r) Z_m{}^i(\lambda r)\right) \cdot \exp[j(m+n)\phi] \exp[-j(\eta+h)z].$$

This is identically zero when integrated with respect to ϕ and z unless $m = -n$ and $\eta = -h$. However, under these conditions, the term in parentheses is identically zero since $\lambda = \Lambda$ when $\eta = -h$. Thus property B follows immediately.

Property C

$$\int_{-\infty}^{\infty}\int_{-\pi}^{\pi} N_{nh}{}^i \times \boldsymbol{M}_{m\eta}{}^j \cdot \hat{r}\, d\phi\, dz = \begin{cases} \dfrac{4\pi^2\Lambda^3}{k} Z_n{}^i(\Lambda r) Z_{-n}{}'^i(\Lambda r)\delta(\eta+h), & \text{for } m = -n \\ 0, & \text{otherwise} \end{cases} \quad \text{(B3)}$$

The integrand of the preceding integral can be simplified as follows:

$$N_{nh}{}^i \times \boldsymbol{M}_{m\eta}{}^j \cdot \hat{r} = -N_{nh}{}^i \cdot (\hat{r} \times \boldsymbol{M}_{m\eta}{}^j) = \frac{\lambda\Lambda^2}{k} Z_n{}^i(\Lambda r) Z_m{}'^i(\lambda r) \cdot \exp[j(m+n)\phi] \exp[j(\eta+h)z].$$

This is zero when integrated with respect to ϕ unless $m = -n$. In this case the integral of the exponential term involving ϕ is 2π. The integral of the exponential term involving z results in the factor $2\pi\delta(\eta+h)$. Since this is zero for $\eta + h \neq 0$, it follows that the substitution $\eta = -h$ can be made in the rest of the expression. Thus property C follows immediately.

Acknowledgment

Without the aid of R. M. Goodman, Chief of the Sensor System Division of the Georgia Institute of Technology Engineering Experiment Station, and J. S. Hollis of Scientific Atlanta Inc., the experimental phase of this work would have been impossible. The authors are grateful for their assistance.

References

[1] D. M. Kerns, "Antenna measurements with arbitrary antennas at arbitrary distances," presented at the High Frequency and Microwave Field Strength Precision Measurements Seminar, National Bureau of Standards, Boulder, Colo., Session 3, Lecture 1, 1966.

[2] R. C. Baird, A. C. Newell, P. F. Wacker, and D. M. Kerns, "Recent experimental results in near-field antenna measurements," presented at the High Frequency and Microwave Field Strength Precision Measurements Seminar, NBS, Boulder, Colo., pp. 349–351, 1966.

[3] E. B. Joy and D. T. Paris, "Spatial sampling and filtering in near-field measurements," *IEEE Trans. Antennas Propagat.*, vol. AP-20, pp. 253–261, May 1972.

[4] J. Brown and E. V. Jull, "The prediction of aerial radiation patterns from near-field measurements," *Proc. Inst. Elec. Eng.*, vol. 108B, pp. 635–644, Nov. 1961.

[5] E. V. Jull, "The prediction of aerial radiation patterns from limited near-field measurements," *Proc. Inst. Eng.*, vol. 110, pp. 501–506, Mar. 1963.

[6] F. Jensen, "Electromagnetic near-field far-field correlations," Ph.D. dissertation, Tech. Univ. Denmark, Lyngby, Denmark, July 1970.

[7] J. R. James and L. W. Longdon, "Prediction of arbitrary electromagnetic fields from measured data," *Alta Freq.*, vol. 38, numero speciale, pp. 286–290, May 1969.

[8] J. A. Stratton, *Electromagnetic Theory*. New York: McGraw-Hill, 1941, pp. 392–395.

[9] W. M. Leach, Jr., "Probe compensated near-field measurements on a cylinder," Ph.D. dissertation, Georgia Inst. Technol., Atlanta, Aug. 1972.

[10] R. F. Harrington, "Effect of antenna size on gain, bandwidth, and efficiency," *J. Res. Nat. Bur. Stand.*, vol. 64D, pp. 1–12, Jan.–Feb. 1960.

[11] R. E. Collin and S. Rothschild, "Evaluation of antenna Q," *IEEE Trans. Antennas Propagat.*, vol. AP-12, pp. 23–27, Jan. 1964.